

3-4-91
E5932

NASA Technical Memorandum 103707

Comparison of Dynamic Fatigue Behavior Between SiC Whisker-Reinforced Composite and Monolithic Silicon Nitrides

Sung R. Choi
Cleveland State University
Cleveland, Ohio

and

Jonathan A. Salem
Lewis Research Center
Cleveland, Ohio

February 1991

NASA

COMPARISON OF DYNAMIC FATIGUE BEHAVIOR BETWEEN SiC WHISKER-
REINFORCED COMPOSITE AND MONOLITHIC SILICON NITRIDES

Sung R. Choi*
Cleveland State University
Cleveland, Ohio 44115

and

Jonathan A. Salem
National Aeronautics and Space Administration
Lewis Research Center
Cleveland, Ohio 44135

SUMMARY

The dynamic fatigue behavior of 30 vol % SiC whisker-reinforced composite and monolithic silicon nitrides were determined as a function of temperature from 1100 to 1300 °C in ambient air. The fatigue susceptibility parameter n decreased from 88.1 to 20.1 for the composite material, and 50.8 to 40.4 for the monolithic, with increasing temperature from 1100 to 1300 °C. A transition in the dynamic fatigue curve occurred for the composite material at a low stressing rate of 2 MPa/min at temperature of 1300 °C, resulting in a very low value of $n = 5.8$. Fractographic analysis showed that glassy phases in the slow crack growth region were more pronounced in the composite compared to the monolithic material, implying that SiC whisker addition promotes the formation of glass rich phases at the grain boundaries, thereby enhancing fatigue. All of these results indicate that SiC whisker addition to Si_3N_4 matrix substantially deteriorates fatigue resistance inherent to the matrix base material for this selected material system.

INTRODUCTION

Ceramics have attracted special interest for high temperature structural applications such as advanced heat engines and heat recovery systems. The major limitation for assuring the reliability of the ceramic materials, however, is their low fracture toughness. The composite approach, in which a low modulus and low strength matrix is reinforced via the incorporation of strong and high modulus SiC whiskers, has shown to be one of the alternatives to improve toughness and strength. Alumina composites reinforced with SiC whiskers have exhibited excellent mechanical properties over their matrix base materials: toughness, strength, and fatigue and thermal shock resistances are substantially higher for the composite materials (refs. 1 to 7).

On the other hand, the composite approach to silicon nitride through SiC whiskers has shown limited success, depending on the fabrication process. It has been demonstrated that the fracture toughness was increased significantly (20 to 30 percent) by the addition of 20 to 30 vol % SiC whiskers, but that the corresponding strength was not significantly improved, or was even lower than the monolithic materials (refs. 8 to 13). Also, composite resistance to impact/erosion, creep and cyclic crack growth has shown some improvement, but

*NASA Resident Research Associate at Lewis Research Center.

in most cases, some deterioration (refs. 14 to 18). The increased processing complexity as well as the high temperature reaction in SiC whiskers are known to be the major cause of such problems.

Although ceramics exhibit retained strength in short-time exposure to high temperature, they are inevitably susceptible to slow crack growth and creep which limit long-term reliability for structural components. In this study, high temperature slow crack growth behavior is described for the GN-10¹ based 30 vol % SiC whisker-reinforced composite and monolithic silicon nitrides. These materials were extensively evaluated previously in terms of strength, fracture toughness, and R-curve behavior (refs. 13 and 19). The results of the previous studies indicated that whisker addition to the Si₃N₄ matrix material did not provide any favorable effect on strength, toughness, and R-curve behavior. In this study we extended the previous work to include slow crack growth behavior of the same composite and monolithic silicon nitride materials. For this purpose, dynamic fatigue was studied in flexure beam specimens as a function of temperatures at 1100, 1200, and 1300 °C in an air environment. An additional dynamic fatigue test was also conducted for comparison with indented specimens at 1100 °C in air.

EXPERIMENTAL PROCEDURES

The materials used in this study were based on the Garrett GN-10 composite and monolithic silicon nitrides. The composite fabrication has been described elsewhere (ref. 13). Briefly, GN-10 silicon nitride powder composition was slip cast into 50 mm diameter, 75 mm height billets, glass encapsulated by the ASEA² method and hot-isostatically pressed to produce monolithic material. Part of the same powder batch was blended with 30 vol % SiC whiskers by ACMC³ and processed with the same procedures as the monolithic material. Densities of the composite and monolithic materials were 3.27 and 3.31 g/cm³, respectively.

The billets of both composite and monolithic materials were cut to produce the flexure test specimens such that the prospective tensile surfaces of the specimens were perpendicular to the billet diameter. All faces of each test specimen were ground to the specimen length with #320 diamond wheels, and the edges were bevelled and then hand-polished with #600 SiC paper lengthwise to minimize spurious failure due to edge effects. The nominal dimension of the test specimens were 2.7 by 4 by 50 mm.

Dynamic fatigue tests for these as-received specimens were conducted in ambient air at three different temperatures of 1100, 1200, and 1300 °C using a fully-articulating four-point bend fixture made of sintered SiC. The inner and outer spans of the bend fixture were 20 and 40 mm, respectively. A preliminary study showed that a loop-shaped load-controlled mode of the testing machine⁴ gave a far better result in applying load to the test specimen during either the heating or testing cycle than the position-controlled mode (constant cross-head speed). The load-controlled mode eliminates a possible excessive load transmitted to the test specimen due to the thermal expansion of loading train

¹Garrett Ceramic Components, Allied Signal, Torrance, CA.

²ABB Autoclave Systems, Columbus, OH.

³Advanced Composite Materials Corp., Greer, SC.

⁴Model 8562, Instron, Canton, MA.

members (push rods, grips, and water-cooled adapters, etc.) caused by temperature difference, thus providing an accurate load application. This is particularly useful for very low stressing rate testing, where a position-controlled mode can not be used because a slight change in temperature in the loading train has a great effect on the crosshead speed. Hence, the load-controlled mode was exclusively used in this study to achieve an accurate loading (or stressing) rate condition. Four loading rates of 2 to 2000 N/min, corresponding to 2 to 2000 MPa/min, were applied at temperatures of 1100 and 1300 °C. At 1200 °C, only two loading rates of 2 and 2000 N/min were employed due to the limited number of specimens. The heating rate of the furnace was kept at 12 °C/min to minimize thermal shock damage to the loading train. Each specimen was preloaded with 20 N to maintain a good alignment of test specimen relative to the testing fixture, and held at test temperature for 20 min prior to testing. The number of the test specimens for each loading rate and a given temperature was three to five. The small number of the specimens (particularly three) was due to the limited availability of the test materials.

For comparison, an additional dynamic fatigue test was carried out with indented specimens (2.7-by 4-by 25-mm bars) at 1100 °C in air. The center of each specimen was indented using an indentation load of 98 N with a Vickers microhardness indenter¹ such that one of the indentation diagonals was aligned normal to the direction of the applied tensile stress. Four loading rates of 4.2 to 4200 N/min, corresponding to the stressing rates of 2 to 2000 MPa/min, were utilized. A four-point SiC bend fixture with spans of 19.0/9.5 mm was used. The number of the test specimens per loading rate was three, which was found to be enough in light of the very small standard deviation (less than 10 percent) of the mean strength.

Fractographic analysis was conducted using optical and scanning electron microscopy to characterize the fracture mode as well as the nature of the flaw origins.

RESULTS AND DISCUSSION

For most ceramics and glasses, the subcritical crack velocity can be approximated by the empirical relation (ref. 20)

$$V = A' \left[\frac{K_I}{K_{IC}} \right]^n = AK_I^n \quad (1)$$

where A' and n are the material/environment constants, K_I and K_{IC} are the Mode I stress intensity factor and fracture toughness, respectively, and $A = A' [K_{IC}]^{-n}$. It should be noted, however, that crack growth behavior under mixed-mode loading differs from that under pure Mode I or pure Mode II loading condition, as noted by Singh and Shetty (ref. 21). For dynamic fatigue testing which employs a constant stressing rate ($\dot{\sigma}$), the corresponding fatigue strength (σ_f) can be readily derived in terms of stressing rate, and the resulting expression is (refs. 22 and 23)

¹Model 3212, Zwick, Germany.

$$\sigma_f^{n+1} = B(n+1)S_i^{n-2}\dot{\sigma} \quad (2)$$

where $B = 2/[AY^2(n-2)K_{IC}^{n-2}]$, S_i is the inert strength, and Y is the crack geometry factor defined in the expression of $K_I = Y\sigma\sqrt{c}$ with σ and c being the applied stress and crack size, respectively. In the same way, the time to failure (t_f) can be obtained as a function of constant applied stress (σ_a) as follows (ref. 23)

$$t_f = BS_i^{n-2}\sigma_a^{-n} \quad (3)$$

From equation (2) it is noted that the fatigue strength decreases with decreasing stressing rate since the crack or crack-like flaws are subjected to more time to grow. The fatigue susceptibility parameters n and B can be obtained, respectively, from the slope and intercept of the dynamic fatigue curve when $\text{Log } \sigma_f$ versus $\text{Log } \dot{\sigma}$ is plotted. Consequently, the parameter A is evaluated from the expression of B in equation (2) with appropriate constants.

A summary of the dynamic fatigue results for the composite and monolithic materials is presented in table I. Included in this table are test temperature, specimen condition, number of specimens, loading rate, stressing rate, number of specimens, and mean fatigue strength. The stressing rate ($\dot{\sigma}$) was calculated using elementary beam theory

$$\dot{\sigma} = \frac{3(L_o - L_i)\dot{P}}{2bh^2} \quad (4)$$

where L_o and L_i are the outer and inner spans of the testing bend fixture, respectively, \dot{P} is the loading rate, and b and h are the specimen width and height, respectively. Note that the time to failure at the lowest stressing rate ($\dot{\sigma} = 2$ MPa/min) was less than 6 hr, and that this duration of time was not long enough to induce any cavitation or microcracks in the tensile surface and a resulting shift of the neutral axis towards the compression side for either material. Therefore, since \dot{P} was constant during testing, the corresponding stressing rate ($\dot{\sigma}$) remained constant even if the materials exhibited limited creep deformation at high temperature.

Table II summarizes the parameters n , B , and A evaluated from experimental data based on equation (2). The values of inert strength (S_i) and fracture toughness (K_{IC}) were taken from the previous studies (refs. 13 and 19): for the composite material, $S_i = 698$ MPa and $K_{IC} = 5.6$ MPa/m; whereas, for the monolithic, $S_i = 732$ MPa and $K_{IC} = 5.6$ MPa/m. The crack geometry factor was taken to be $Y = 1.13$ assuming that the strength-controlling flaws are those with half penny-shaped configuration.

Figure 1 shows the dynamic fatigue results of the as-received composite specimens, where median fatigue strengths (σ_f) are plotted as a function of applied stressing rates ($\dot{\sigma}$) at three different temperatures of 1100 to 1300 °C.

The decrease in fatigue strength with decreasing stressing rate is evident indicating that slow crack growth occurred at all the test temperatures used. The fatigue susceptibility parameter n decreases from 88.1 to 20.1 as the corresponding temperature increases from 1100 to 1300 °C, which indicates that fatigue susceptibility increases very rapidly with increasing temperature.

It is also important to note from figure 1 that a transition in the dynamic fatigue curve occurs at the lowest stressing rate of $\dot{\sigma} = 2.0$ MPa/min at 1300 °C, resulting in a very low value of $n = 5.8$. The transition was primarily attributed to creep that was enhanced by a combination of both the high temperature and the very slow deformation rate. Evidence of creep deformation at this stressing rate can be seen in figure 2, where deflection of the test specimen is plotted against distance from the one end of the specimen. Also, a deflection curve of the specimen tested at a fast stressing rate of $\dot{\sigma} = 2000$ MPa/min is included for comparison. It can be seen from this figure that creep deformation at $\dot{\sigma} = 2$ MPa/min is significant and about six times greater than that at $\dot{\sigma} = 2000$ MPa/min. A similar observation to this transition is also found in a study of the static fatigue behavior of alumina reinforced with 20 percent SiC whiskers at a temperature of 1200 °C in ambient air (ref. 6). It should be emphasized here that such transition should be taken into account when reliability and lifetime analysis are made for the structural components, as mentioned by Fett and Munz (ref. 24).

The results of the dynamic fatigue test with the monolithic material are presented in figure 3. As seen in the case for the composite materials (fig. 1), the fatigue strength decreases with both decreasing stressing rate and increasing temperature. However, the fatigue parameter n decreases monotonically from 50.8 to 40.4 with increasing temperature from 1100 to 1300 °C. In contrast to the case for the composite material, the monolithic material exhibited no "transition" in the dynamic fatigue curve at 1300 °C. However, some limited creep deformation, although much less than exhibited by the composite specimens, was still observed at this temperature from the specimens tested at a very low stressing rate of $\dot{\sigma} = 2$ MPa/min.

The effect of temperature on the fatigue behavior of the two materials can be seen more clearly in figure 4, where both the fatigue parameters n and A are plotted as a function of temperature. At 1100 °C, the fatigue parameter n of the composite is higher than that of the monolithic; while, from 1200 °C the situation is reversed, resulting in lower n for the composite than the monolithic material. For the fatigue parameter A , the composite exhibited a lower A than the monolithic at low temperature (1100 °C); however, at temperatures ≥ 1200 °C, the parameter A is greater for the composite compared to the monolithic. This result indicates that the temperature dependence of the fatigue parameters n and A is very strong for the composite compared to the monolithic counterpart. Since the higher n and lower A gives better fatigue resistance (or less fatigue susceptibility), it can be concluded that resistance to fatigue at temperatures ≥ 1200 °C is much greater for the monolithic than the composite material. This means that whisker addition to the matrix Si_3N_4 did not provide any favorable effect on fatigue resistance for this chosen material system, as was the case for the strength, toughness and R-curve behavior (refs. 13 and 19). Actually, whisker addition resulted in substantial deterioration of the fatigue resistance inherent to the matrix base material.

For the indentation cracks, healing occurred in the monolithic specimens at the low stressing rate of $\dot{\sigma} < 20$ MPa/min, yielding an unusually high n value. Therefore, the fatigue result for the indented monolithic specimens was not included in the analysis. Results of the dynamic fatigue test for the indented composite specimens at 1100 °C in air are presented in figure 5. For comparison, the fatigue curve of the as-received specimens is included. The obtained fatigue parameter $n = 50.8$ for the indented specimens is lower than that ($n = 88.1$) obtained from the as-received specimens. In other words, the fatigue resistance of the inherent flaws is greater than that of the artificial flaws produced by indentation. This result indicates that fatigue behavior of well-defined cracks is somewhat different from that of the inherent flaws, as seen in the fatigue data for the indented Si_3N_4 by Guan et al. (ref. 24). It is believed that the inherent flaws have a less defined crack configuration compared to the indent crack, thereby resulting in a more deviated crack propagation behavior as compared to indent cracks.

A convenient way to show the effects of fatigue is to construct a lifetime prediction diagram in conjunction with levels of failure probability. In this section, a simple lifetime prediction will be described based on the experimental data in order to statistically compare fatigue behavior of the two materials. The strength distribution of a brittle material is generally expressed with a two parameter Weibull function of $\text{Ln Ln} [1/(1 - F)] = m \text{Ln}(S_i/S_0)$, where F is the failure probability, and m and S_0 are the Weibull modulus and scale parameter, respectively. By solving for S_i from this Weibull function and substituting into equation (3), one can obtain the following time-to-failure equation as a function of failure probability (ref. 23)

$$\text{Ln } t_f = \text{Ln } B + \frac{n - 2}{m_i} \text{Ln Ln} \frac{1}{1 - F} + (n - 2) \text{Ln } S_{0i} - n \text{Ln } \sigma_a \quad (5)$$

where m_i and S_{0i} are, respectively, the Weibull modulus and scale parameter in inert (room temperature) strength distribution. One of the potential limitations in applying equation (5) to structural components, e.g., heat engines, is that external flaw population could be altered at high temperature via flaw healing and flaw nucleation processes due to oxidation or other environmental attack. In this case, the crack growth, flaw healing, and flaw generation should be first quantified so that the combined failure probability, and the total time to failure can be estimated, as noted by Ritter et al. (ref. 26). This requires complete characterization of the combined effects of fatigue, flaw healing and flaw nucleation on strength, which is beyond the scope of this paper. In this analysis, however, we assumed for simplicity that initial flaw population is unchanged at high temperature and that high temperature strength is solely determined by one mechanism, that is, slow crack growth of the initial flaws that control the room temperature strength distribution. Evans suggested that this fracture mechanics principle, equation (1), is also applicable at high temperature even when limited creep deformation is exhibited (ref. 27).

In view of equation (5), lifetime prediction requires reliable data on the inert strength distribution of test samples. Unfortunately, reliable room-temperature Weibull strength data of the current composite and monolithic materials was not available in the previous study (ref. 13) due to the limited number of test specimens (typically less than 10). However, Weibull modulus and scale parameter were estimated approximately using the statistical reproducibility analysis proposed by Ritter et al. (ref. 28).

$$m_i \approx \frac{1.2}{C.V} \quad (6a)$$

$$S_{oi} \approx \frac{S}{\Gamma\left(1 + \frac{1}{m_i}\right)} \quad (6b)$$

where C.V is the coefficient of variation of the mean strength, S is the mean strength, and Γ is the gamma function. Now using the room temperature strength values (ref. 13) of $S = 698 \pm 85$ and $S = 732 \pm 61$ MPa, respectively, for the composite and monolithic, one can obtain: $m_i = 9.8$ and $\text{Ln } S_{oi} = 6.599 \text{ Ln(MPa)}$ for the composite; $m_i = 14.4$ and $\text{Ln } S_{oi} = 6.632 \text{ Ln(MPa)}$ for the monolithic. Despite the insufficient number of the test specimens, the estimated Weibull modulus, however, is in a good agreement with the typical range of $m_i \approx 7$ to 15 commonly observed for sintered silicon nitride materials at room temperature. It can also be seen that the estimated values of $m_i = 14.4$ and $\text{Ln } S_{oi} = 6.632 \text{ Ln(MPa)}$ for the monolithic material compares very well with $m_i = 16.6$ and $\text{Ln } S_{oi} = 6.624 \text{ Ln(MPa)}$ that were evaluated from a linear regression analysis of the actual strength data, as shown in figure 6. Note that the number of the test specimens in this figure is limited to eight.

Using the estimated m_i and S_{oi} from equation (6) together with the previously evaluated n and B constants (table II), a lifetime prediction curve was constructed based on equation (5), and is given in figure 7. Here, the prediction was made for failure probability of $F = 10^{-4}$ and 10^{-1} at 1300 °C. For the composite material, $n = 20.1$ was used. This figure clearly illustrates that there exists great difference in fatigue behavior between the two materials. At the high applied stress and low failure probability (10^{-4}), difference in lifetime between the two materials is small. However, with decreasing applied stress and increasing failure probability, the difference becomes greater, resulting in much shorter lifetime for the composite compared to the monolithic material. To ensure a lifetime of 1 year, for example, the applied stresses should be 103 and 217 MPa, respectively, for composite and monolithic materials for the failure probability of $F = 10^{-4}$; whereas, for $F = 10^{-1}$, the applied stresses should become 196 and 344 MPa, respectively, for the composite and monolithic. If the lower value of $n = 5.8$, for the purpose of conservative estimation of lifetime, is used for the composite material, the applied stress should be decreased to the factor of 10 from the case of $n = 20.1$ to ensure the same lifetime of 1 year. Although limited experimental data and simplistic technique for analyzing the statistical data were used in this prediction, this result shows again that fatigue resistance of the monolithic material is superior to the composite counterpart for this chosen material system.

Examination of the fracture surfaces of the two materials that failed at temperature ≤ 1200 °C showed that most failures originated from surface porous regions, coarse grain regions and agglomerates. However, at the temperature of 1300 °C, the flaw origins were not generally discernible since the fracture surfaces were covered with glassy phases probably due to oxidation. The slow crack growth phenomenon was not observed directly from the fractographs of the specimens failed at 1100 °C due to the limited slow crack growth (note that fatigue parameter n at 1100 °C is greater than 50 for both materials). A typical example of fracture surface for the monolithic specimen failed at

1100 °C is shown in figure 8, where the fracture mirror and the flaw origin associated with surface porous region are clearly seen.

The slow crack growth phenomenon can be observed more easily from the specimens that failed at the increased temperature of 1300 °C, especially for the specimens tested at the low stressing rate of $\dot{\sigma} = 2$ MPa/min. Figure 9 shows a comparison of the fracture surfaces of the composite specimens tested at two different stressing rates of $\dot{\sigma} = 2$ and 2000 MPa/min at 1300 °C. At a high stressing rate of $\dot{\sigma} = 2000$ MPa/min, the amount of slow crack growth is insignificant; whereas, at the low stressing rate of $\dot{\sigma} = 2$ MPa/min the crack growth becomes more dominant, which is reflected from the fatigue strength data shown in figure 1. It was found that fracture surfaces were heavily covered with viscous glassy phases. These glassy phases in the slow crack growth region could be the result of long time exposure to high temperature air and then surface oxidation. Also, note the appearance of rough surface in the slow crack growth region. The mode of fracture in this region is thus believed intergranular, which is a characteristic of slow crack growth.

The glassy phases on the slow crack growth region was observed to be more severe in the composite than monolithic material, as shown in figure 10. It is believed that this abundance of the glassy phases in the composite material was due to silica on the surface of the whiskers. The addition of silica to glassy phases already present at the grain boundaries could result in easier separation of grains and cause rapid crack growth, thereby enhancing fatigue. Based on the experimental results on fatigue strength and fractographic analysis, it is inferred that the enhanced fatigue behavior observed in the composite material over the monolithic is attributed to more severe formation of glassy phases at the crack tip. Nixon et al. (ref. 16) in their study of creep behavior on SiC whisker reinforced silicon nitrides also showed that more silica formed in the whisker-matrix interfaces, thus resulting in inferior creep resistance for the composite material. Further study using analytical method (e.g., TEM) is needed to understand in more details fatigue behavior of the composite material.

CONCLUSIONS

The fatigue susceptibility parameter n for the composite Si_3N_4 decreased rapidly from 88.1 to 20.1 with increasing temperature from 1100 to 1300 °C. A transition in the dynamic fatigue curve occurred in the composite material at 1300 °C at the lowest stressing rate of $\dot{\sigma} = 2$ MPa/min, resulting in a very low value of $n = 5.8$. This transition was ascribed to creep enhanced by a combination of both the high temperature and the very low deformation (stressing) rate. For the monolithic material, the fatigue parameter n decreased monotonically from 50.8 to 40.4 with increasing temperature from 1100 to 1300 °C. In contrast to the composite, the monolithic material did not exhibit a transition in the dynamic fatigue curve at 1300 °C. It was also observed that the temperature dependence of fatigue parameter A is much greater in the composite than the monolithic material. Fractographic analysis showed that more glassy phase formed in the slow crack growth region of the composite as compared to the monolithic, implying that SiC whisker addition promoted the formation of glass rich phases at the grain boundaries which in turn enhanced

fatigue. All of these results show that whisker addition to Si_3N_4 matrix material deteriorates fatigue resistance inherent to the matrix base material for this selected material system. This contrasts with the results of a previous study (ref. 19), where no appreciable difference in high temperature strength, toughness, and R-curve behavior existed between the composite and monolithic materials.

ACKNOWLEDGMENT

The authors are grateful to R. Pawlik for the extensive high temperature experiments and SEM work during the course of this study.

REFERENCES

1. Becher, P.F.; and Wei, G.C.: Toughening Behavior in SiC-Whisker-Reinforced Alumina. *J. Am. Ceram. Soc.*, vol. 67, no. 12, Dec. 1984, pp. 267-269.
2. Wei, G.C.; and Becher, P.F.: Development of SiC-Whisker-Reinforced Ceramics. *Am. Ceram. Soc. Bull.*, vol. 64, no. 2, Feb. 1985, pp. 298-304.
3. Homeny, J.; Vaughn, W.L.; and Ferber, M.K.: Processing and Mechanical Properties of SiC-Whisker- Al_2O_3 -Matrix Composites. *Am. Ceram. Soc. Bull.*, vol. 66, no. 2, Feb. 1987, pp. 333-338.
4. Lio, S., et al.: Mechanical Properties of Alumina/Silicon Carbide Whisker Composites. *J. Am. Ceram. Soc.*, vol. 72, no. 10, Oct. 1989, pp. 1880-1884.
5. Tiegs, T.N.; and Becher, P.F.: Thermal Shock Behavior of a Alumina-SiC Whisker Composite. *J. Am. Ceram. Soc.*, vol. 70, no. 5, May 1987, pp. C-109-C-111.
6. Becher, P.F., et al.: Elevated-Temperature-Delayed Failure of Alumina Reinforced with 20 Vol % Silicon Carbide Whiskers. *J. Am. Ceram. Soc.*, vol. 73, no. 1, Jan. 1990, pp. 91-96.
7. Becher, P.F., et al.: Toughening Behavior in Whisker-Reinforced Ceramic Matrix Composites. *J. Am. Ceram. Soc.*, vol. 71, no. 12, Dec. 1988, pp. 1050-1061.
8. Campbell, G.H., et al.: Whisker Toughening: A Comparison Between Alumina Oxide and Silicon Nitride Toughened with Silicon Carbide. *J. Am. Ceram. Soc.*, vol. 73, no. 3, Mar. 1990, pp. 521-530.
9. Shalek, P.D., et al.: Hot-Pressed SiC Whisker/ Si_3N_4 Matrix Composites. *Am. Ceram. Soc. Bull.*, vol. 65, no. 2, Feb. 1986, pp. 351-356.
10. Buljan, S.; Baldoni, J.G.; and Huckabee, M.L.: Si_3N_4 -SiC Composites. *J. Am. Ceram. Soc.*, vol. 66, no. 2, Feb. 1987, pp. 347-352.

11. Pezzotti, G., et al.: Processing and Mechanical Properties of Dense Si_3N_4 -SiC-Whisker Composites without Sintering Aids. *J. Am. Ceram. Soc.*, vol. 72, no. 8, Aug. 1989, pp. C-1461-C-1464.
12. Lundberg, R., et al.: SiC-Whisker-Reinforced Si_3N_4 Composites. *Am. Ceram. Soc. Bull.*, vol. 66, no. 2, Feb. 1987, pp. 330-333.
13. Salem, J.A.: Strength and Toughness of Monolithic and Composite Silicon Nitrides. NASA TM-102423, 1990.
14. Ritter, J.E.; Choi, S.R.; and Jakus, K.: Erosion Testing of High Tech Ceramics and Metals. Unpublished work, University of Massachusetts, 1989.
15. Akimune, Y.; Katano, Y.; and Matoba, K.: Spherical-Impact Damage and Strength Degradation in Silicon Carbide Whisker/Silicon Nitride Composites. *J. Am. Ceram. Soc.*, vol. 72, no. 5, May 1989, pp. 791-798.
16. Nixon, R.D., et al.: Steady-State Creep of Hot-Pressed SiC Whisker-Reinforced Silicon Nitride. *Compos. Sci. Technol.*, vol. 37, no. 1-3, 1990, pp. 313-328.
17. Baldoni, J.G.; and Buljan, S.T.: Creep and Crack Growth Resistance of Silicon Nitride Composites. *Ceramic Materials and Components for Engines; Proceedings of the Third International Symposium, Las Vegas, NV, Nov. 27-30, 1988*, V.J. Tennery, ed., American Ceramic Society, Inc., 1989, pp. 786-795.
18. Suresh, S.; Han, L.X.; and Petrovic, J.J.: Fracture of Si_3N_4 -SiC Whisker Composites under Cyclic Loads. *J. Am. Ceram. Soc.*, vol. 71, no. 3, Mar. 1988, pp. C-158-C-161.
19. Choi, S.R.; and Salem, J.: Strength, Toughness and R-Curve Behaviors of SiC Whisker-Reinforced Si_3N_4 with Reference to Monolithic Si_3N_4 . Submitted for publication to *J. Mater. Sci.*, 1990.
20. Evans, A.G.; and Wiederhorn, S.M.: Proof Testing of Ceramic Materials - An Analytical Basis for Failure Prediction. *Int. J. Fract.*, vol. 10, Sept. 1974, pp. 379-392.
21. Singh, D.; and Shetty, D.K.: Subcritical Crack Growth in Soda-Lime Glass in Combined Mode I and Mode II Loading. *J. Am. Ceram. Soc.*, vol. 73, no. 12, Dec. 1990, pp. 3597-3606.
22. Evans, A.G.: Slow Crack Growth in Brittle Materials under Dynamic Loading Conditions. *Int. J. Fract.*, vol. 10, 1974, pp. 251-259.
23. Ritter, J.E.: Engineering Design and Fatigue Failure of Brittle Materials. *Fracture Mechanics of Ceramics, Vol. 4*, R.C. Bradt, D.P.H. Hasselman, and F.F. Lange, eds., Plenum Publishing Corporation, New York, 1978, pp. 667-686.

24. Fett, T.; and Munz, D.: Lifetime Prediction for Hot-Pressed Silicon Nitride at High Temperatures. Methods for Assessing the Structural Reliability of Brittle Materials, ASTM STP-844, S.W. Freiman and C.M. Hudson, eds., American Society for Testing and Materials, Philadelphia, PA, 1984, pp. 154-176.
25. Guan, Z.D.; and Liu, W.J.: High Temperature Creep Cracking Behavior with an Advanced Method for Data Treatment. Ceramic Materials and Components for Engines; Proceedings of the Third International Symposium, Las Vegas, NV, Nov. 27-30, 1988, V.J. Tennery, ed., American Ceramic Society, Inc., 1989, pp. 796-805.
26. Ritter, J.E., et al.: Application of Fracture Mechanics in Assessing Against Fatigue Failure of Ceramic Components. Ceramics for High-Performance Application III: Reliability, E.M. Leno, R.N. Katz, and J.J. Burke, eds., Plenum Publishing Corp., New York, 1983, pp. 503-533.
27. Evans, A.G.: High-Temperature Slow Crack Growth in Ceramic Materials. Ceramics for High-Performance Applications; Proceedings of the Second Army Materials Technology Conference, Hyannis, MA, Nov. 13-16, 1973, J.J. Burke, A.E. Gorum, and R.N. Katz, eds., Brook Hill, Chestnut Hill, MA, 1974, pp. 373-396.
28. Ritter, J.E.; Bandyopadhyay, N.; and Jakus, K.: Statistical Reproducibility of the Dynamic and Static Fatigue Experiments. Am. Ceram. Soc. Bull., vol. 60, no. 8, Aug. 1981, pp. 798-806.

TABLE I. - SUMMARY OF DYNAMIC FATIGUE RESULTS OF COMPOSITE AND MONOLITHIC SILICON NITRIDES

Temperature, °C	Specimen condition	Loading rate, P, N/min	Stressing rate, $\dot{\sigma}$, MPa/min	Composite			Monolithic		
				Number of specimen	Fracture strength		Number of specimen	Fracture strength	
					σ_f , MPa	(a)		σ_f , MPa	(a)
1100	As-received	2	2	5	598.9	63.1	3	609.2	35.1
↓		20	20	↓	584.5	82.0	4	649.0	45.3
↓		200	200	↓	615.9	54.8	3	675.3	41.8
↓		2000	2000	↓	641.5	33.8	4	697.4	5.1
1200		2	2	4	463.0	106.4	3	537.2	48.4
↓		2000	2000	4	558.9	19.5	4	621.5	63.4
↓		2	2	4	318.0	4.8	↓	513.3	49.3
↓		20	20	3	445.2	44.2	↓	523.3	47.3
↓		200	200	3	487.6	48.5	↓	596.4	75.1
↓		2000	2000	4	553.9	38.0	↓	591.4	21.0
1100	Indented	4.2	2	3	351.5	4.8	-	-----	-----
↓		42	20	↓	353.1	11.3	-	-----	-----
↓		420	200	↓	372.4	11.1	-	-----	-----
↓		4200	2000	↓	400.5	26.9	-	-----	-----
↓				↓			-	-----	-----

^aThese numbers indicate ± 1.0 standard deviation.

TABLE II. - SUMMARY OF FATIGUE PARAMETERS OF COMPOSITE AND MONOLITHIC SILICON NITRIDES

Fatigue parameters	Temperature, °C					
	1100		1200		1300	
	Composite	Monolithic	Composite	Monolithic	Composite	Monolithic
n	88.1	50.75	35.7	46.37	^a 20.1/ ^b 5.8	40.43
Ln B, MPa ² min	-1.0219	6.0924	.2809	.5762	^a 3.9784	.4346
Ln A, m/min	-151.31	-93.51	-61.40	-86.05	^a -39.58	-75.62

^aThe parameters evaluated based on $\dot{\sigma} = 2000, 200, \text{ and } 20 \text{ MPa/min.}$

^bThe parameters evaluated based on $\dot{\sigma} = 20 \text{ and } 2 \text{ MPa/min.}$

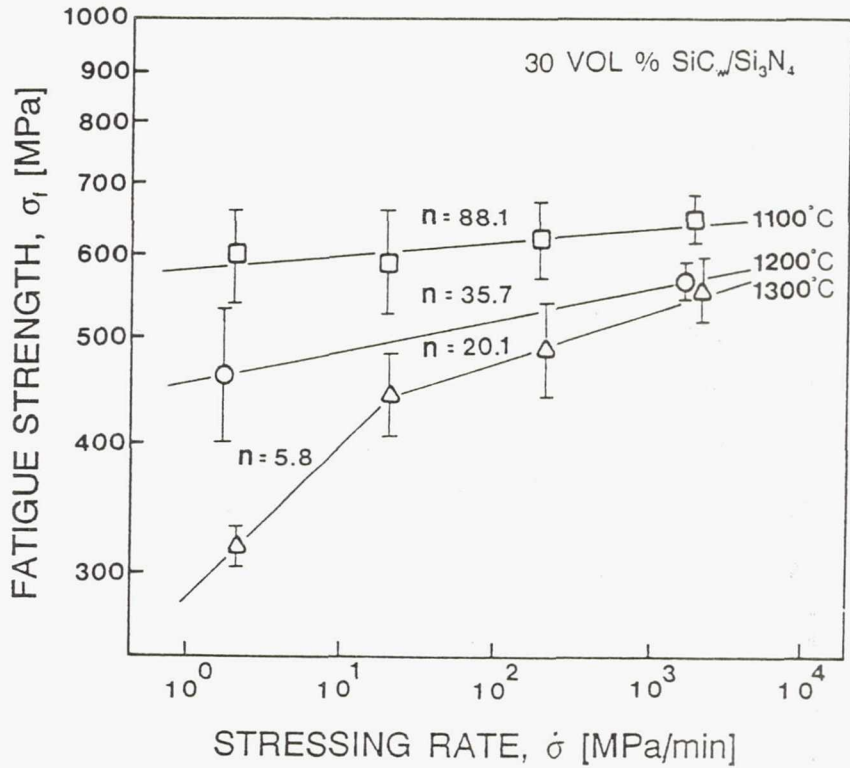


Figure 1.—Dynamic fatigue results for 30 vol % SiC whisker-reinforced Si₃N₄ at temperatures of 1100, 1200 and 1300 °C in ambient air. Error bar indicates ± 1.0 standard deviation.

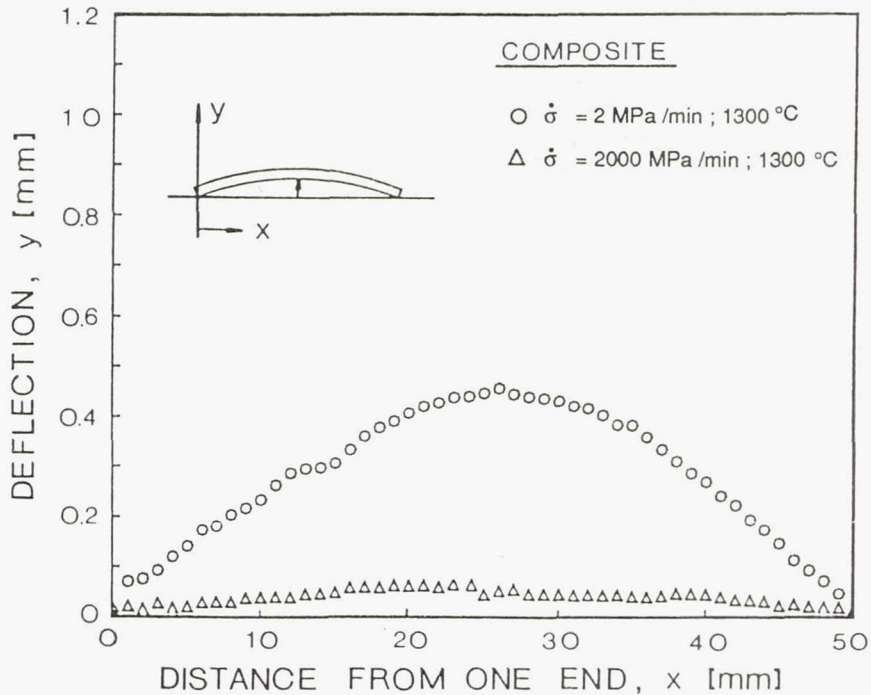


Figure 2.—Deflection curves of the composite specimens tested at stressing rates of $\dot{\sigma} = 2$ and 2000 MPa/min at 1300 °C.

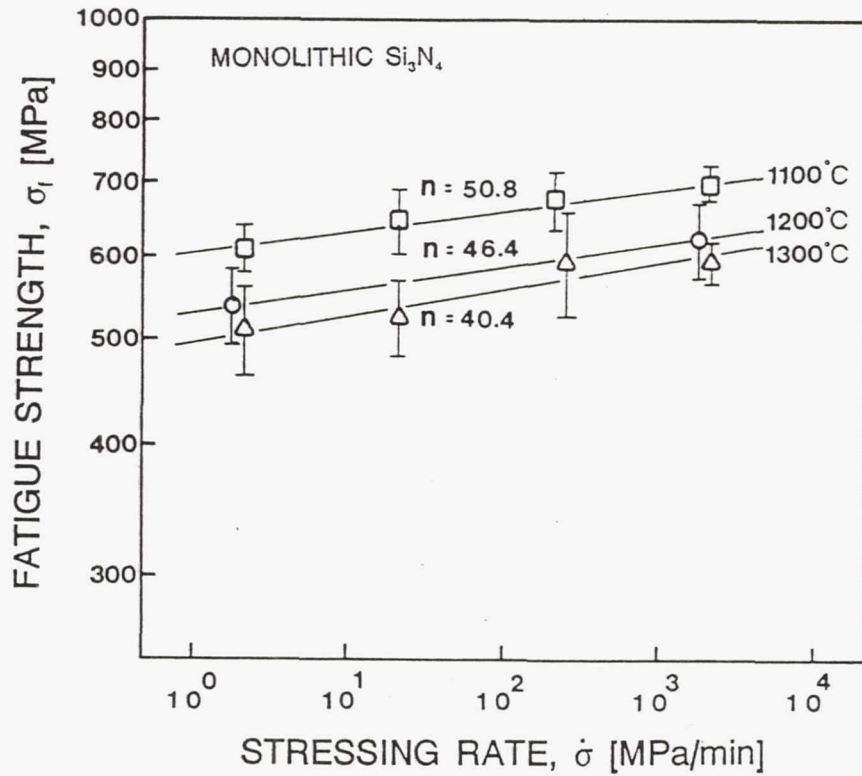
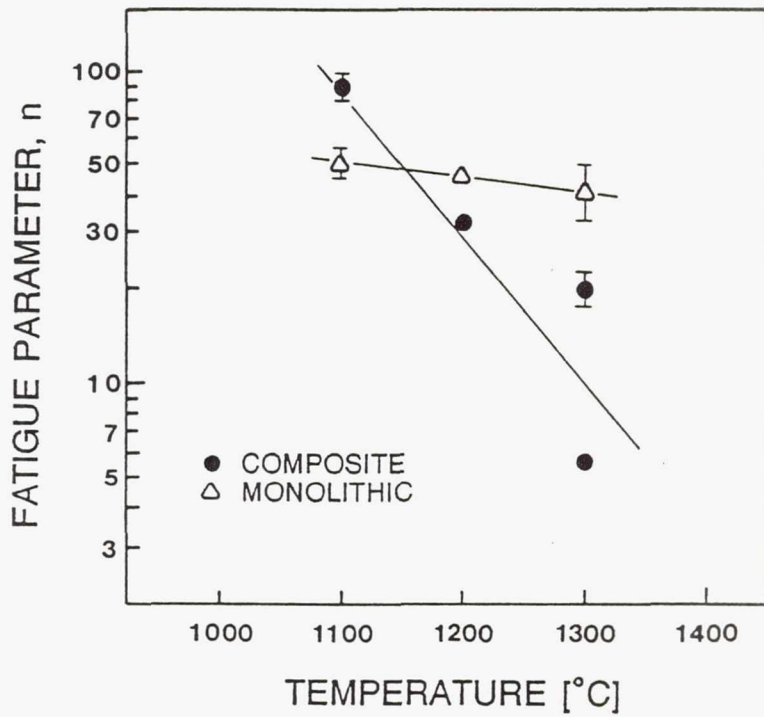
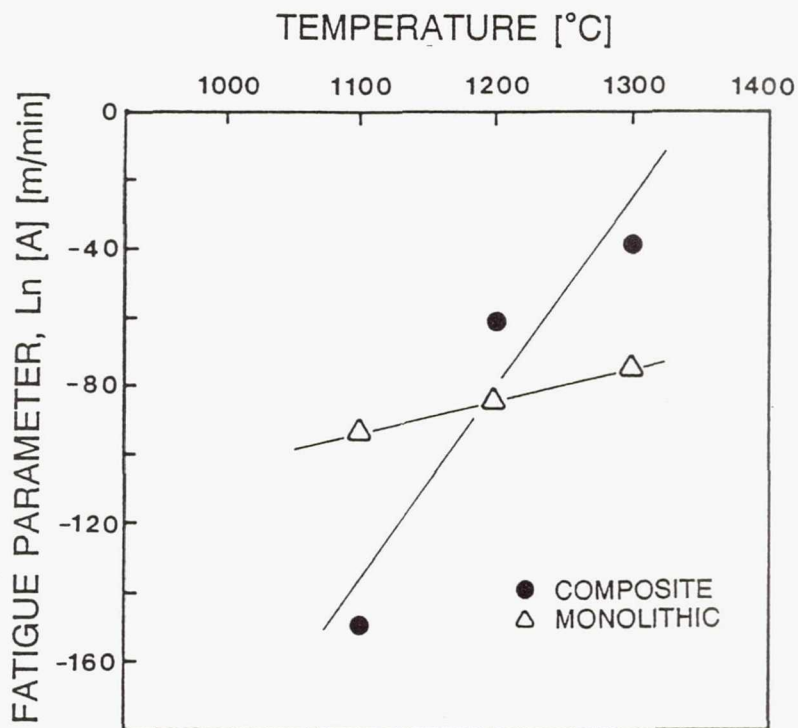


Figure 3.—Dynamic fatigue results for monolithic Si_3N_4 at temperatures of 1100, 1200 and 1300 C in ambient air. Error bar indicates ± 1.0 standard deviation.



(a) n. For the composite material the fatigue parameter n for the transition region ($\dot{\sigma} \leq 20$ MPa/min) is also presented.



(b) A.

Figure 4.—Plots of fatigue parameters n and A as a function of temperature for composite and monolithic Si_3N_4 's.

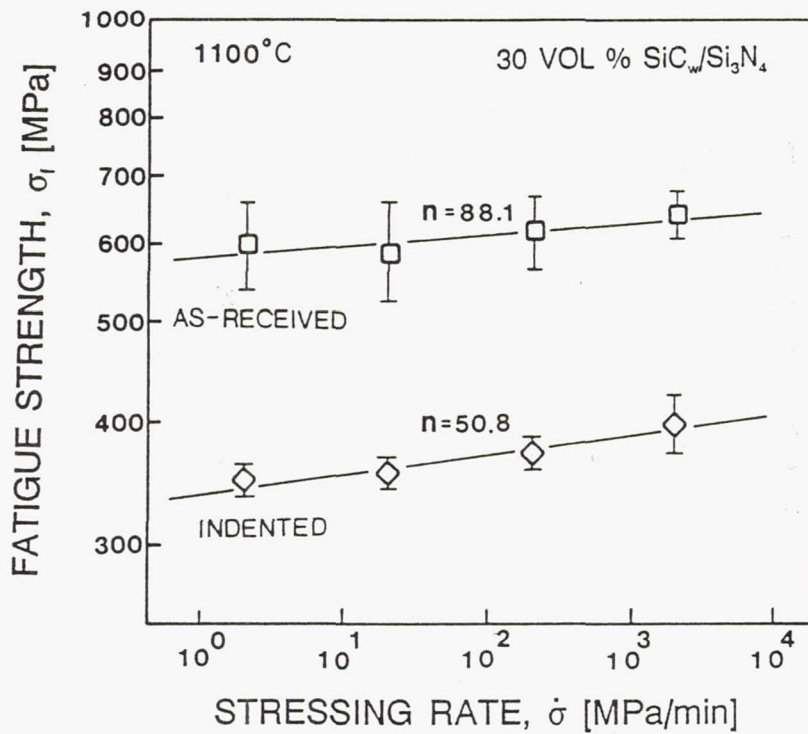


Figure 5.—Comparison of dynamic fatigue data of the composite Si₃N₄ between indented and as-received specimens. Test temperature was 1100 °C, and indent load employed was 98 N.

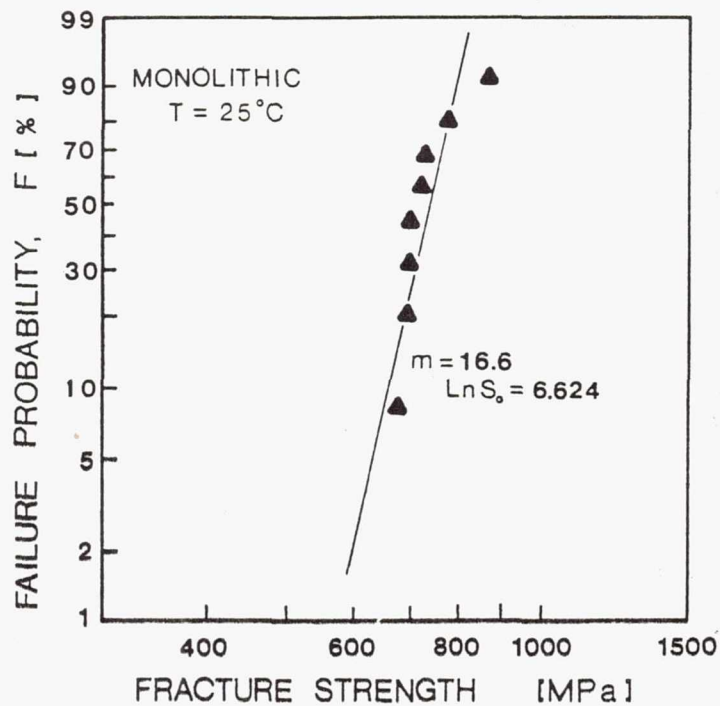


Figure 6.—Weibull strength distribution for the monolithic Si₃N₄ specimens tested at room temperature (Data from Ref. 13.).

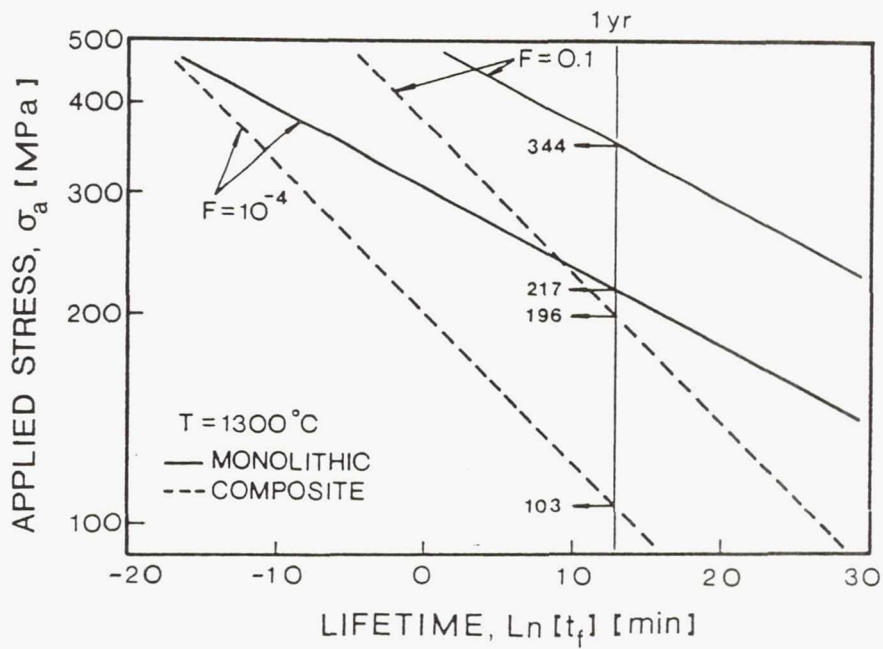
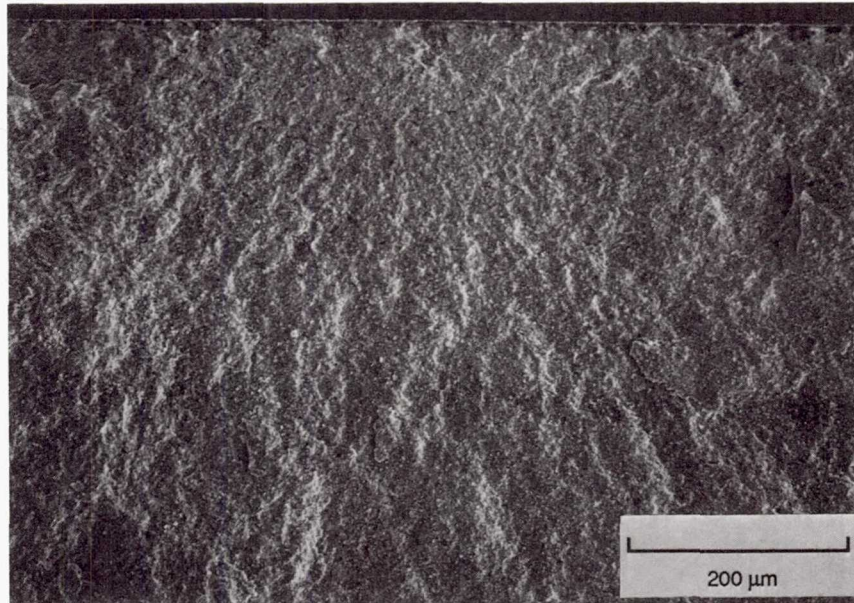
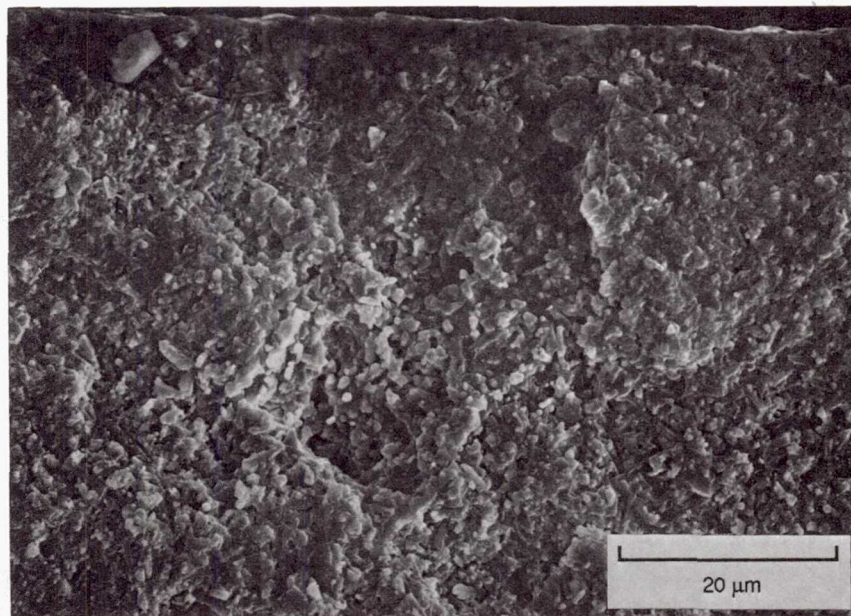


Figure 7.—Lifetime prediction diagram for the composite and monolithic Si_3N_4 's for the two different levels of failure probabilities of $F = 10^{-1}$ and 10^{-4} at 1300°C . The fatigue parameter of $n = 20.1$ was used for the composite Si_3N_4 .

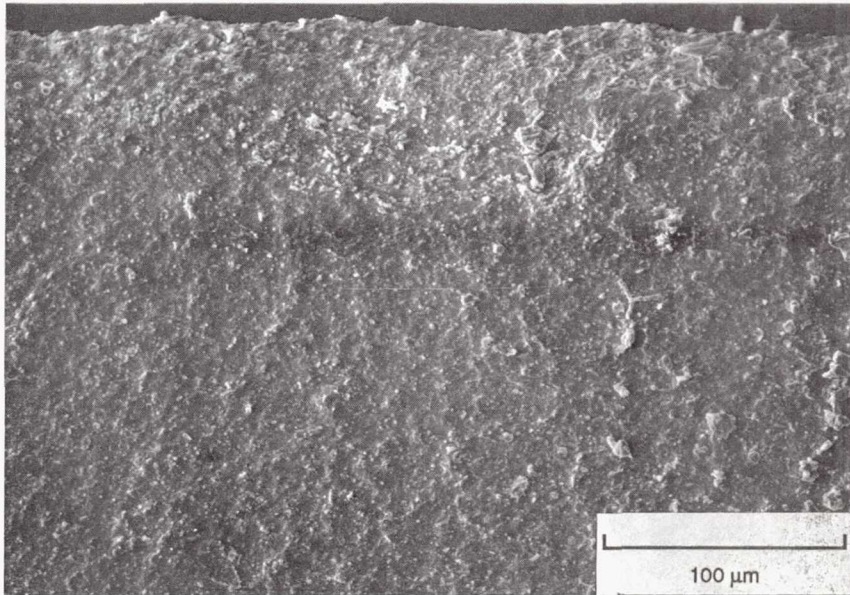


(a) Overall view.

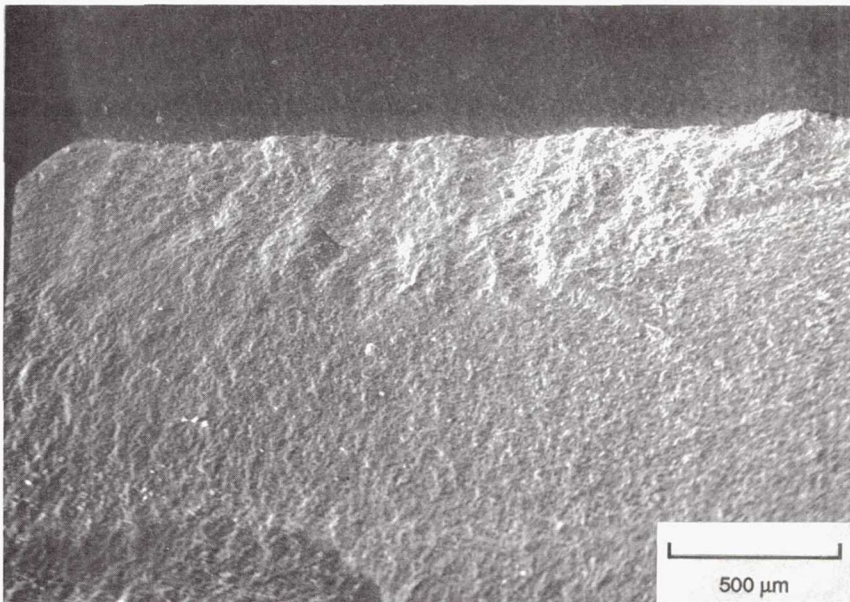


(b) Enlarged view of the failure origin showing that failure was associated with subsurface porous region.

Figure 8.—A typical example of SEM fractographs of the monolithic specimen failed at $\dot{\sigma} = 2$ MPa/min at 1100 °C. Note that the amount of slow crack growth was very limited at this temperature.

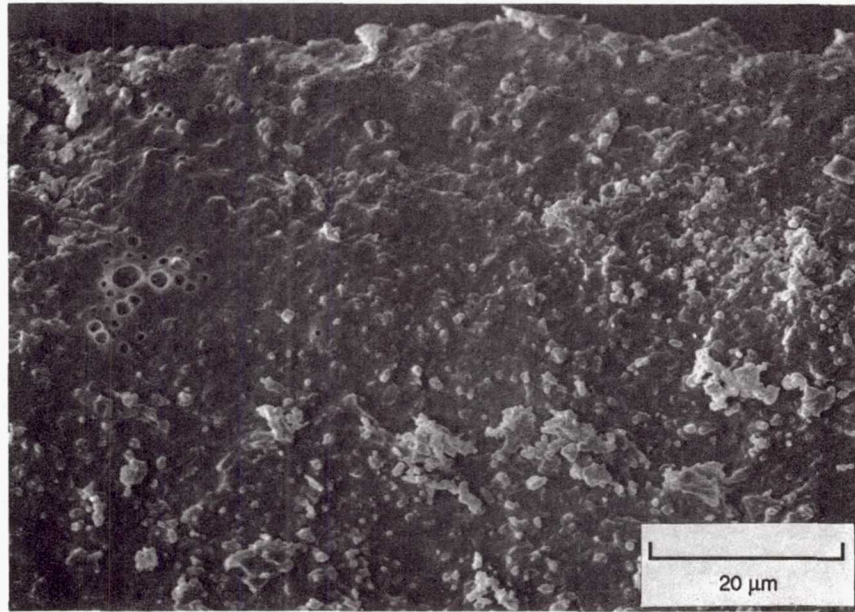


(a) The slow crack growth region of a specimen tested at $\dot{\sigma} = 2000$ MPa/min.

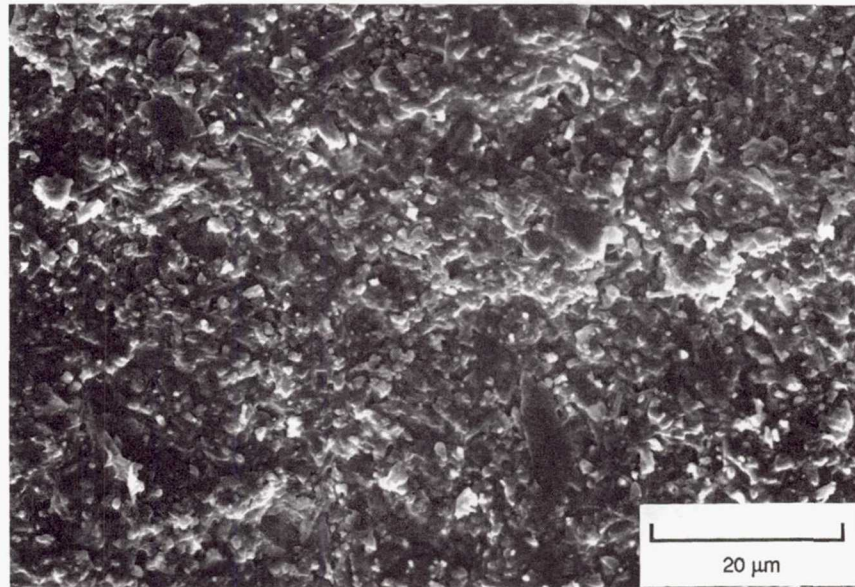


(b) The slow crack growth region of a specimen tested at $\dot{\sigma} = 2$ MPa/min.

Figure 9.—SEM fractographs of the composite specimens failed at high and low stressing rates at 1300 °C. Note the dependence of slow crack growth on stressing rate.



(a) Composite specimen.



(b) Monolithic specimen.

Figure 10.—SEM fractographs showing degree of the glassy phases on fracture surfaces between composite and monolithic specimens. Both specimens were tested at $\dot{\sigma} = 2000$ MPa/min at 1300 °C.

1. Report No. NASA TM-103707		2. Government Accession No.		3. Recipient's Catalog No.	
4. Title and Subtitle Comparison of Dynamic Fatigue Behavior Between SiC Whisker-Reinforced Composite and Monolithic Silicon Nitrides				5. Report Date February 1991	
				6. Performing Organization Code	
7. Author(s) Sung R. Choi and Jonathan A. Salem				8. Performing Organization Report No. E-5932	
				10. Work Unit No. 505-63-1M	
9. Performing Organization Name and Address National Aeronautics and Space Administration Lewis Research Center Cleveland, Ohio 44135-3191				11. Contract or Grant No.	
				13. Type of Report and Period Covered Technical Memorandum	
12. Sponsoring Agency Name and Address National Aeronautics and Space Administration Washington, D.C. 20546-0001				14. Sponsoring Agency Code	
15. Supplementary Notes Sung R. Choi, NASA Resident Research Associate and Cleveland State University, Cleveland, Ohio 44115; Jonathan A. Salem, NASA Lewis Research Center. Responsible person, Sung R. Choi, (216) 433-8366.					
16. Abstract The dynamic fatigue behavior of 30 vol % SiC whisker-reinforced composite and monolithic silicon nitrides were determined as a function of temperature from 1100 to 1300 °C in ambient air. The fatigue susceptibility parameter n decreased from 88.1 to 20.1 for the composite material, and 50.8 to 40.4 for the monolithic, with increasing temperature from 1100 to 1300 °C. A transition in the dynamic fatigue curve occurred for the composite material at a low stressing rate of 2 MPa/min at temperature of 1300 °C, resulting in a very low value of n = 5.8. Fractographic analysis showed that glassy phases in the slow crack growth region were more pronounced in the composite compared to the monolithic material, implying that SiC whisker addition promotes the formation of glass rich phases at the grain boundaries, thereby enhancing fatigue. All of these results indicate that SiC whisker addition to Si ₃ N ₄ matrix substantially deteriorates fatigue resistance inherent to the matrix base material for this selected material system.					
17. Key Words (Suggested by Author(s)) Dynamic fatigue; SiC Whisker-reinforced silicon nitride; Monolithic silicon nitride; Lifetime prediction; High temperature slow crack growth			18. Distribution Statement Unclassified - Unlimited Subject Category 27		
19. Security Classif. (of this report) Unclassified		20. Security Classif. (of this page) Unclassified		21. No. of pages 22	22. Price* A03